Effect of cell-size on the energy absorption features of closed-cell aluminium foams

S. K. Nammi [*a], G. Edwards [b] and H. Shirvani [a]

[a] Anglia Ruskin University, Marconi 215, CM1 1SQ, UK

[b] Department of Electronic & Electrical Engineering, Faculty of Science and Engineering, Thornton Science Park, University of Chester, Pool Lane, Ince, Chester, CH2 4NU, UK

Abstract:

The effect of cell-size on the compressive response and energy absorption features of closed-cell aluminium (Al) foam were investigated by finite element method. Micromechanical models were constructed with a repeating unit-cell (RUC) which was sectioned from tetrakaidecahedra structure. Using this RUC, three Al foam models with different cell-sizes (large, medium and small) and all of same density, were built. These three different cell-size pieces of foam occupy the same volume and their domains contained 8, 27 and 64 RUCs respectively. However, the smaller cell-size foam has larger surface area to volume ratio compared to other two. Mechanical behaviour was modelled under uniaxial loading. All three aggregates (3D arrays of RUCs) of different cell-sizes showed an elastic region at the initial stage, then followed by a plateau, and finally, a densification region. The smaller cell size foam exhibited a higher peak-stress and a greater densification strain comparing other two cell-sizes investigated. It was demonstrated that energy absorption capabilities of smaller cell-size foams was higher compared to the larger cell-sizes examined.

Keywords:

Aluminium foam, Cell-size, Energy absorption, Repeating unit-cell, Micromechanical

*corresponding author, E-mail: sathish.nammi@anglia.ac.uk

Nomenclature:

Al	Aluminium
TKD	Tetrakaidecahedra
RUC	Repeating Unit-Cell
SAF	Stabilized Aluminium Foam
SEM	Scanning Electron Microscope
ρ^*	Density of foam
ρ_s	Density of intrinsic material of foam
σ	Nominal stress
ε	Nominal strain
ε_d	Densification strain
σ_{pl}^*	Plateau stress
t	Cell-wall (pore) thickness
l	Cell edge-length of TKD foam
$3D$	Three-dimensional
L_x	End-to-end distance in global x direction of TKD foam
L_y	End-to-end distance in global y direction of TKD foam
L_z	End-to-end distance in global z direction of TKD foam
E^*	Elastic modulus of foam
E_s	Elastic modulus of intrinsic material modulus of foam
E_V	Energy absorbed per unit-volume
S	Surface area of foam
V	Volume of foam

1. Introduction

Cellular solids are widespread in nature. They are made of arrays of small enclosed spaces that are also referred to as cells. Examples include a bee's honeycomb, cork, sponge, and trabecular bone.Closed-cell Al foams are man-made artificial cellular solids that have many applications in aerospace, automotive, biomedical and engineering industries in general [1-3]. Al foams can be used in the area of blast energy absorption and crashworthiness and protection against Micro-Meteoroid and Orbital Debris (MMOD) particle impacts in space engineering [4]. They have the ability to absorb kinetic energy from impact and can delay and attenuate stress waves in a typical explosion [5, 6]. Al foams have the ability to undergo plastic deformation at a nearly constant stress level, over a wide range of strain. This makes them ideal for energy absorption. Sandwich panels made of Al foam core can be used as lightweight crash pads.

Cellular structures of real Al foams are complex; each individual cell is different to others in size and shape forming a disordered solid on the mesoscale. Additionally, material distribution within an individual cell is non-uniform. Typical cellular geometry of real closed-cell foam is shown in Figure 1. Note that the terminology *real* will be used throughout in this work to represent manufactured foams. It is far too challenging to model three-dimensional representations capturing all cell features of real Al foam. Numerical modelling techniques that involve complex features such as corrugations, curvature and voids require impractical computational effort. Thus, idealization of geometry is carried-out to minimize computational effort. Simplified micromechanical models consider the geometry to be homogeneous, akin to a crystalline lattice, making it possible to characterize and quantify behaviour. Cellular solids characterization is mainly carried-out in three length scales (viz: macro-, meso-, and micro) [7]. Modelling at the macro level examines global behaviour (or collective characteristics of material) of whole system of foam cells. Al foam is described with a homogeneous material behaviour. i.e. a constitutive law is employed to generate yield criterion for foams [8]. On the other hand, at micro-scale modelling, the behaviour of the individual cell constituents such as voids, corrugations, plateau edges and imperfections etc. need to be accounted for. The macro and micro scale characterizations are also referred to as phenomenological and micro-mechanical modelling respectively. The meso-scale is modelling is intermediate between the aforementioned. Repeating Unit-Cell (RUC) based modelling is often used in both micro and meso scales [9].

The foam specimen dimension relative to the cell-sizes is important in order to apply the constitutive models effectively; the overall specimen size has to be at least greater by order of 10 than the dimensions of a single foam cell [10]. On the other hand, micromechanical models are the only solutions available to predict general foam behaviour when some dimensions of Al foam section are of a few cell diameters. Thus, the micromechanical models are mainly used for identifying optimum conditions for best mechanical properties. In this respect, the work described here will go some way in the design of microstructure for better energy absorption. Specifically, investigations are focussed here on Al foams of three different cell-sizes with the same density.

2. Problem statement

Cell-sizes of real Al foam can be controlled to a certain extent. begging the question on how cell-size effects the energy absorption features of same density Al foam. The issue to be considered is

whether smaller cells (with thin cell-walls) or larger cells (with thick cell-walls) have better energy absorption characteristics . From materials design view point of view, this knowledge is precursor in the design of a blast resistant casing that uses Al foam as a sacrificial energy absorber as shown in Figure 2. A strip (end-to-end thickness 25.4 mm) of real Al foam of density (ρ^*) 0.17 g/cm^3 is sandwiched between two steel layers as shown in Figure 2. The thickness of outer layer of steel (i.e. facing blast load) can be varied whilst the inner layer is made of 18 gauge steel body. Depending on the foam cell-size, a thickness of 25.4 mm cross-section of foam can be filled with between 2 to 4 cell diameters. It is obviously possible to increase the number of cells if the Al foam is filled with smaller cells. However, cost considerations and technological challenges mean that between 2 to 4 cells are practical. From the design point of view, the sandwiched Al foam must absorb the blast energy without damaging the contents in casing.

3. Compressive response and energy absorption features

Closed-cell real Al foam of density 0.17 g/cm^3 were obtained from CYMAT Corporation [11]. Intrinsic Al material was assumed to have a density (ρ_s) 2.7 g/cm^3. An experimental stress (σ)-strain (ε) plot of this Al foam under compression is shown in Figure 3. The compressive response of Al foam consists of three regions (Linear-elastic, Plateau and Densification). The initial linear-elastic region is considerably shorter. The second region exhibits almost constant plateau for lower density foams. Higher density foams exhibit a gradual rise in plateau. The plateau region is predominantly employed in energy absorption applications. In the third stage, Al foams show a rapid rise in load for minimal increment in strain. The strain at which this occurs is referred to as densification strain (ε_d). All foams exhibit these three regions of stress-strain behaviour due to their underlying cellular structure. For efficient energy absorption, the plateau stress (σ_{pl}^*) of the Al foam chosen is to be as close as the blast pressure generated. From the compressive response plot, the plateau stress is determined using the relation:

$$\sigma_{pl}^* = \frac{\int_0^{\varepsilon_d} \sigma \, d\varepsilon}{\varepsilon_d} \tag{1}$$

4. Unit-cell based foam

The cell-wall thickness of Al foam specimens of density 0.17 g/cm^3 were measured using SEM. A typical image of foam pore (cell-wall) is shown in Figure 4. A strong variation in cell-wall thickness was noticed for cells. Radii of curvatures (plateau region) at the interconnection of network of cells has maximum pore thickness. An average pore thickness (t) of 99 μm was computed according to the method adopted by Simone and Gibson [12]. TKD based micromechanical models were constructed [13] based on identified cell-wall thickness. A diagram of RUC in TKD is shown in Figure 5. The RUC shown in Figure 6 has a cell edge-length l, and occupies a volume equal to $4l \times 2\sqrt{2}l \times 4l$. The end-to-end distance of this RUC in both global x and z directions are $4l$, whereas it is $2\sqrt{2}l$ in y direction. The density of foam is calculated according to the relation:

$$\frac{l}{t} = \frac{1.1837}{\rho^*/\rho_s} \tag{2}$$

Three foam models of different size RUCs that occupy the same volume (3D space) were created with 8, 27 & 64 unit-cells respectively. All foam models were of identical relative density (0.17 g/cm^3) even though the cell-wall thickness (t) and cell-edge length (l) of the RUCs used in each is different. The aggregates of RUCs (3D array) with 8, 27 & 64 cells will be referred to as large, medium and small respectively. All three aggregates of different cell-sizes are shown in Figure 7. A pore thickness (t) of 99 μm identified for a representative density of 0.17 g/cm^3 was assigned to aggregate of 64 RUCs (small cell aggregate). Its edge-length (l) of 1861.2 μm was obtained from equation (2) for small cell RUC. The large and medium cell-size foam models were further constructed by varying l and t. In order to obtain the cell wall thickness for medium and large unit-cells, the small cell wall thickness was extrapolated by factors of 33.3 and 100% respectively, while keeping the relative density constant. Thus, the cell wall thicknesses obtained for medium and large cells were 132 μm and 198 μm respectively. By inputting the wall-thickness and relative density parameters into the equation (2), the edge-lengths obtained for medium and large cells were 2481.59 μm and 3722.38 μm respectively. The aggregate of 64 small RUCs occupies 3D space (volume) equivalent to $16l \times 8\sqrt{2}l \times 16l$ which is equivalent to $29779 \times 21057 \times 29779$ μm^3. The aggregates of 8 large and 27 medium RUCs also have the same volume and aspect ratio ($\frac{l}{t} = 18.8$). The size of TKD unit-cell is directly dependent on its edge-length (l). The individual size of the RUC used in 64 cells aggregate was smaller compared with the 27 medium cell size aggregate. Similarly, the RUC size for the 8 cell aggregate was larger than its counterpart 27 medium cell cell size aggregate . The edge-lengths of medium and large RUCs are longer compared with the smaller cell.

5. FE modelling

Two separate crush simulations were carried-out. In the first analysis, using the implicit procedure, elastic moduli was computed. In the second analysis, the explicit procedure was used to simulate compressive response. Elastic moduli of all three cell arrays were evaluated in both x and y directions. This was compared with theoretical results. The x and z directions are equivalent for the TKD foam model so the foam properties along x and z are also identical. After model verification, the cell aggregates were subjected to large-strain and energy absorption analysis. Particular emphasis was placed on energy absorption features. The FE code ABAQUS [14] was used in the numerical calculations presented here. Al foam models were sandwiched in between a fixed and a movable rigid surface. An illustration of this set-up with loading in the principal x direction, for all the three cell aggregates, is shown in Figure 8. A similar set-up was used for y directional loading, as illustrated for a 64 small RUC aggregate in Figure 9.

ABAQUS reference points were defined for each rigid surface and their motion were effectively controlled by assigning a rigid wall boundary condition. All displacement degrees of freedoms were set to be zero for the fixed rigid surface, via constraining the relevant reference point. The movable rigid surface was constrained to translate only in the direction of applied velocity. All other translational degrees of freedom were restricted except in the direction of predefined velocity. The energies and accelerations were controlled so as to achieve a quasi-static solution. , The computed movable rigid surface displacement and computed reaction force outputs were obtained. This output data was further processed to obtain stress-strain plots.

Contact interactions were defined between the rigid surfaces and foam. The rigid surfaces were defined as master and the foam as slave. A friction free self-contact type algorithm was used for all foam elements in order to prevent the interpenetration of cell walls during the crushing. All models were simulated for two different types of contact interactions, the rough and frictional. The contact interactions prevent foam models from sliding laterally to the direction of loading. Both penalty and kinematic types of mechanical constraint formulations were used between master and slave. All simulations were repeated so as to achieve consistent results. The unit-cells were assigned with AA5182 Al alloy material data in Table 1. The mechanical properties used here came from uniaxial tensile tests on dog-bone specimens. For the initial static analysis (implicit method) only elastic properties were used whereas complete stress-strain data was used for large-strain crush simulations. The cell walls were discretized with shell (S4R type ABAQUS) elements. Five integration points were used over the thickness for each finite element. These shell elements are best suited for the FE analysis which involves the thickness of cell-walls less than $1/10$ of the characteristic length of element. For the simulated RUC foam, the cell-edge length to cell-wall thickness ratio was maintained between 20 and 38.5. The S4R is a 4-node quadrilateral type element, with hourglass control capabilities. These are suitable for large-strain crush analysis involving buckling and severe bending of shells.

5.1. Verification of FE models

A static analysis was carried-out to compute the relative moduli of all three foam models in both x and y directions. Rigid surfaces were assigned with displacement boundary conditions. For x directional loading, a deformation to induce 0.1% strain was applied to the reference point connected to the movable rigid surface. At the same time, the lateral directional (along y and z axes) translational degrees of freedom (DOF) for this reference point were restricted from movement. For example, the end-to-end distance of the global x direction (L_x) is $16l$ for 64 small unit-cells aggregate. A strain of 0.1% for L_x with an edge-length (l) of 1861.2 μm is equivalent to 29.7792 μm. When these displacement boundary conditions were given to the movable rigid surface, it induces a reaction force at both rigid surfaces. The stress was computed by dividing this reaction force by the tributary area. Since, this stress is for a small induced deformation, the ratio of stress to strain can be taken as the effective modulus. Then, the relative modulus (E^*/E_s) can be obtained by dividing the effective modulus (E^*) with the intrinsic material modulus (E_s).

The tributary area is the area cutting the foam system on a plane. For example, when l is the edge-length for each unit-cell, then the effective span of $4 \times 4 \times 4$ small RUCs aggregate in the global y and z directions are given as $L_y = 8\sqrt{2}l$ and $L_z = 16l$ respectively. The product of these two lengths, given by $A = L_y \times L_z = 128\sqrt{2}l^2$ is taken as the tributary area of small cell aggregate for calculating the x directional modulus. Similarly, for the y directional loading, the tributary area is $256l^2$. Whatever the cell edge-lengths for extra-small, small, medium and large unit-cells, their tributary areas are same for all three types of aggregates investigated here, it is approximated as $627056087.5\mu m^2$ and $886791223.3\,\mu m^2$ for x & y directional loadings. When a movable rigid surface is subjected to a displacement, it renders reaction forces. By dividing the reaction force by the tributary area, the stress was obtained which was then divided by the strain to obtain elastic

modulus. Simone and Gibson [15] have developed an equation for the relative modulus of TKD lattice with crystallographic axis (110), which is given by:

$$\frac{E^*}{E_s} = 0.3325\left(\frac{\rho^*}{\rho_s}\right) + 0.3116\left(\frac{\rho^*}{\rho_s}\right)^2 \quad (3)$$

The relative density (ρ^*/ρ_s) of Al foam investigated here is approximately 0.06296. Hence, the theoretical relative modulus (E^*/E_s) as per equation (4) is equivalent to 0.02217. In Figure 10, the FE analysis based results for all three cell-sizes were compared with theoretical results. The relative moduli of aggregates of for the 64 small, 27 medium RUCs are within 2.3% of theoretical result thus verifying the FE models.

6. Results and discussion

The stress-strain plot responses were analysed for peak-stress and energy absorption features. The effect of contact conditions on the compressive responses was also investigated. The cell-size effects on the energy absorption features were also characterised. The sensitivity of stress-strain response to both rough and frictional types of contact interaction properties were also studied. The deformable foam was assigned as slave, whereas the stiffer rigid surfaces were treated as master. Models were simulated under a default coulomb frictional coefficient of 0.1 for the contact frictional formulation. All simulations were repeated for two types of mechanical constraint enforcement methods (Penalty and Kinematic) in ABAQUS FE code. Model responses were found to be almost identical whatever the contact method.

6.1. Stress-strain plots

All three cell-size aggregates produced a flat-topped curve in the neighbourhood of peak-load independent of loading direction. Computed stress-strain plot characteristics were qualitatively similar in shape as that of real Al foam. Note that micromechanical models in literature [16 - 18] in many cases exhibited a stiff initial response with a peak-load, with a significant steep-drop, whereas, the current models are closer to the experimentally observed response of Al foam. TKD based RUC models of Al foam produced simulation results with the three regions of the stress – strain curve under compression. All three dissimilar cell-size aggregates, keeping the same density, have broadly similar shapes. However, there were variations in the position of peaks and valleys in the plateau phase. Compressive response for x directional loading is shown in Figure 11. The peak-stress value of foam with smaller unit-cells was noted to be higher compared to larger cell-aggregates. The strain at which this peak-stress is reached was lower for small unit-cell aggregate. The average plateau stress of the large unit-cell aggregate was higher compared to other two (small and medium) aggregates. Also, the third region of steeply rising stress started at a larger strain, for smaller unit-cell foam. The peak-stress was almost 10% higher for small cell aggregates compared to its larger cell counterpart. However, the difference in peak-stress between medium and small cell-size aggregates is very small. This suggests that the there exists a threshold cell-size beyond which any reduction in size do not significantly affect peak-stress values.

Compressive responses for 64 small RUC aggregate models for both x and y directional loading are shown in Figure 12. The plateau phase response for y directional loading is smooth while it is oscillatory with peaks and valleys, for x directional loading. Also, there are differences in the onsets of plateau and densification stages. The densification stage starts early for y directional loading. Within the linear-elastic phase, the responses were almost identical. However, the non-linear features and the peak-stress at the onset of buckling showing minor variations suggesting a relatively low level of anisotropy in two principal directions. The average plateau stress for both loading directions is similar. FE models consistently showed an oscillatory plateau phase with differences in locations of peaks and valleys for each aggregate. This is independent of the number of cells used, while the trend for positions of local minimum and maximum features were comparable. For x directional loading on small RUC aggregate, the difference between first peak and valley was higher compared to the subsequent oscillations. The first peak and valley corresponds to the collapse of first layer of cells. The oscillatory response show a decay in amplitude although the distance between two consecutive peaks remained nearly the same. However, the average crush force was fairly constant during the entire crushing process.

6.2. Energy absorption characteristics

Stress-strain plots were further analysed for energy absorption characteristics. The energy absorbed per unit-volume (E_V) were computed for all three aggregates. The energy absorbed per unit volume, up to a strain ε, is defined as:

$$E_V = \int_0^{\varepsilon} \sigma(\varepsilon)\, d\varepsilon \tag{3}$$

Here $\sigma(\varepsilon)$ is the instantaneous stress corresponding to instantaneous strain ε. Energy absorbed per-unit volume (E_V) for all three aggregates for x directional loading is shown in Figure 13. The E_V of both medium and small unit-cell aggregates versus strain are almost same. The densification strain for medium size cell-aggregates is 3-5% lower compared to smaller-cell aggregate. For a strains of 10 and 30%, the E_V values of small unit-cell aggregate is greater by 7.4% and 12.2% respectively compared to larger 8 RUC aggregates.

FE investigations show that smaller cell Al foam constructed with thin cell-walls exhibit greater mechanical strength compared to larger-cells of same density. The 8 unit-cells aggregate exhibited a lower peak-stress compared to 27 or 64 cell aggregates. However, the increase in peak-stress between medium and small cell-size was not significant. This apparent higher strength can be explained by observing the surface area to volume ratio (S/V) of foam systems. The surface area to volume ratio (S/V) for 64 small unit-cells model was higher compared to the 27 medium and 8 large cells, which is shown in Figure 14.

7. Summary

The work described here gives an insight into how cell-size affects the mechanical and energy absorption properties. The RUC of TKD foam model calculations displayed three stages (linear-elastic, plateau and densification) of stress-strain response, mimicking real Al foam behaviour. Aggregates of three different RUCs (small, medium and large) of same density and volume have showed broadly different results for peak-stress, energy absorption features and densification

strains. Smaller cell-size foam showed a greater energy absorption features and higher peak-stresses. This is likely due to the fact that the moving rigid-wall was resisted to a greater extent by a foam having more evenly distributed network of small cells. A correlation between surface area to volume ratio (S/V) and the mechanical properties was noted. The final regime of steeply rising stress in the stress – strain curve for smaller unit-cell aggregate, initiates at a larger strain compared to larger cell foam.

Acknowledgments

The authors acknowledge support of CYMAT Corporation for providing AL foam. This work was also partially supported by the European Commission under RECONASS (FP7-312718), a collaborative project part of the Seventh Framework Programme for research, technological development and demonstration. Further-more, authors would like to thank all the partners of the consortium for their valuable contribution.

References

[1] F. García - Moreno, Commercial applications of metal foams: their properties and production, Materials 9 (2) (2016) 85.

[2] J. Banhart, Manufacture, characterisation and application of cellular metals and metal foams, Progress Mater. Sci. 46 (6) (2001) 559–632.

[3] D. Schwingel, H. W.Seeliger, C. Vecchionacci, D. Alwes, J. Dittrich, Aluminium foam sandwich structures for space applications, Acta Astronaut.61 (1–6) (2007) 326–330, ISSN0094-5765.

[4] S. Ryan, T. Hedman, E. L. Christiansen, Honeycomb vs. foam: evaluating a potential upgrade to International Space Station Module Shielding for Micro meteoroids and Orbital Debris, Technical Report. NASA Center for Aerospace Information, NASA/TM-2009-214793, 2009.

[5] M. D. Goel, Ph. Altenhofer, V. A. Matsagar, A. K. Gupta, Ch. Mundt, S. Marburg, Interaction of a shock wave with a closed cell aluminium metal foam,Combust. Explos. Shock Waves 51 (3) (2015) 373–380.

[6] R. P. Merrett, G. S.Langdon , M. D. Theobald, The blast and impact loading of aluminium foam, Mater. Des. 44 (2013) 311–319.

[7] H. P. Degischer, B. Kriszt, Handbook of Cellular Metals: Production, Processing, Applications, Wiley-VCH Verlag GmbH &Co. KGaA, Weinheim, 2002, ISBN 3-527-60055-8.

[8] C. Chen, T. J. Lu, A phenomenological framework of constitutive modelling for incompressible and compressible elasto-plastics solids, Int. J. Solids Struct. 37 (2000) 7769 – 7786.

[9] F. G. Rammerstorfer, D. H. Pahr, T. Daxner, W. K. Vonach, Buckling in thin walled micro and mesostructures of light weight materials and material compounds Comput. Mech.37 (6) (2006) 470 - 478.

[10] P. R. Onck, E. W. Andrews, L. J. Gibson, Size effects in ductile cellular solids. Part I: modeling, Int. J. Mech. Sci. 43 (2001) 681 – 699.

[11] Cymat Technologies Ltd, ⟨http://www.cymat.com⟩, 6320 Danville Rd, Mississauga, ON. L5T2L7.

[12] A. E. Simone, L. J. Gibson, Aluminium foams produced by liquid-state processes, Acta Mater. 46 (9) (1998) 3109 – 3123.

[13]S. K. Nammi, P. Myler, G. Edwards. Structural impact study of “ideal” 3D aluminium foam, in: Proceedings of Salford Postgraduate Annual Research Conference 2010 (SPARC10), pp.238 – 246, ISBN: 978-1-4477-8072-4.

[14]ABAQUS Numerical code. Abaqus Analysis User's Manuals, Simulia, Dassault Systemes, Rising Sun Mills, 166 Valley Street, Providence, RI 02909 - 2499, USA.

[15] A. E. Simone, L. J. Gibson, Effects of solid distribution on the stiffness and strength of metallic foams, Acta Mater. 46 (6) (1998) 2139 - 2150.

[16] S. Santosa , T. Wierzbicki, On the modelling of crush behaviour of a closed-cell aluminum foam structure, J. Mech. Phys. Solids 46 (4) (1998) 645 – 669.

[17] S. A .Meguid, S. S. Cheon, N. El-Abbasi, FE modelling of deformation localization in metallic foams, Finite Elem. Anal. Des. 38 (2002) 631 – 643.

[18] A. Czekanski, M. S. Attia, S .A. Meguid, M. A. Elbestawi, On the use of a new cell to model geometric asymmetry of metallic foams, Finite Elem. Anal. Des. 41 (2005)1327 – 1340.

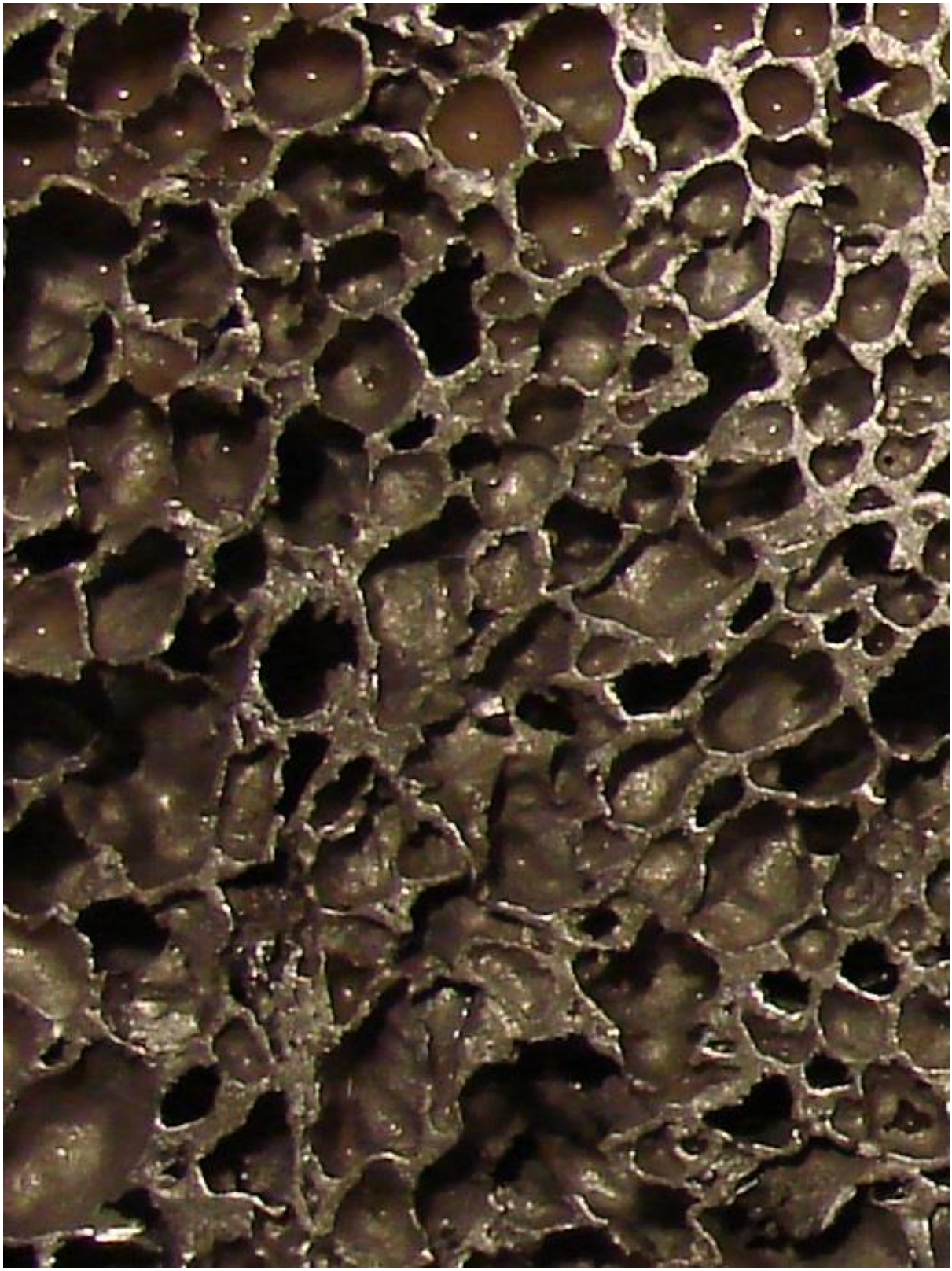

Figure 1 Cellular structure of Al foam

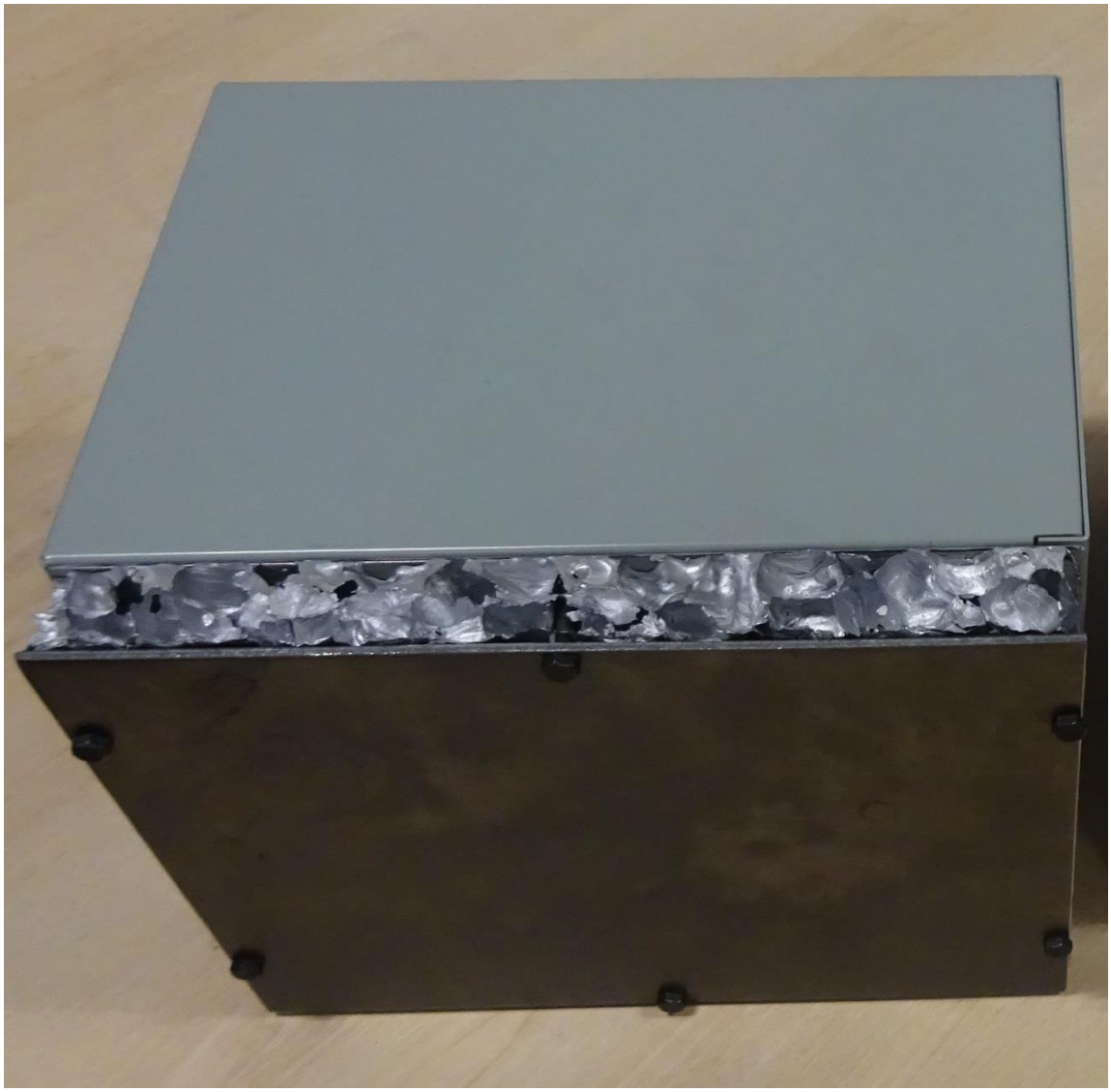

Figure 2 Al foam reinforced casing

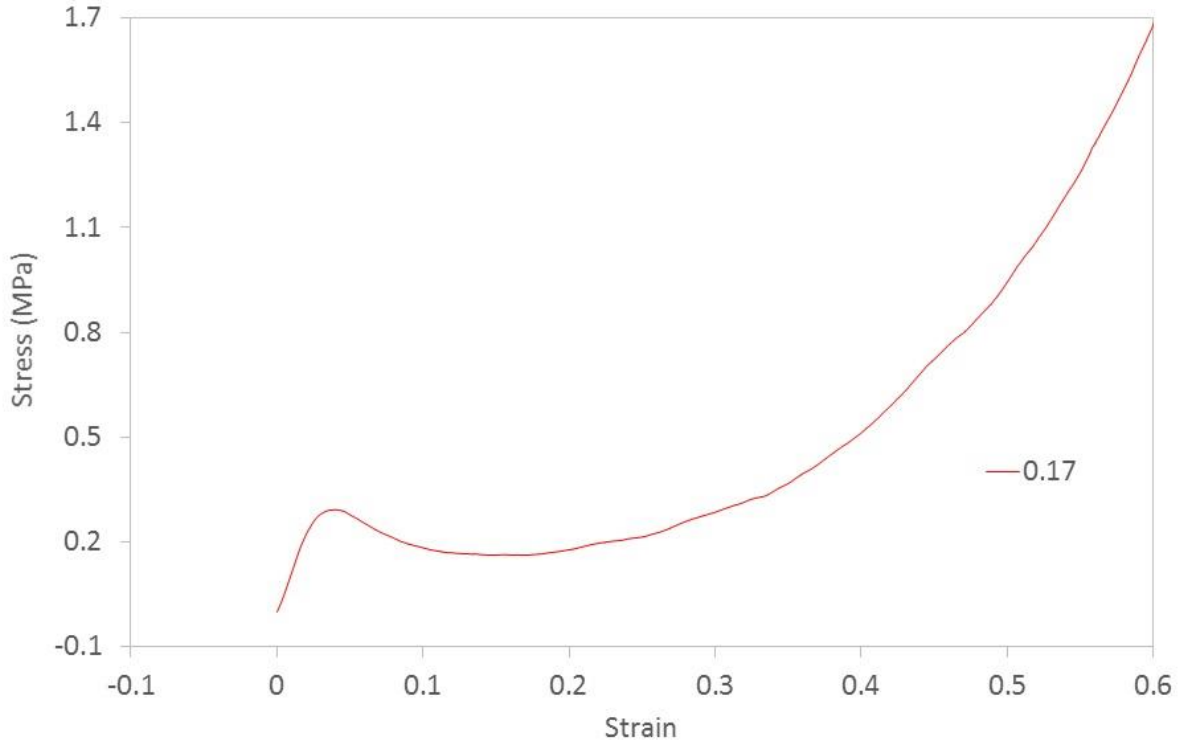

Figure 3 Experimental stress-strain plot of Al foam in compression

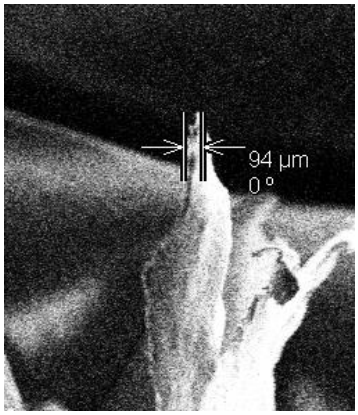

Figure 4 Illustration of pore (cell-wall) thickness measurement under SEM

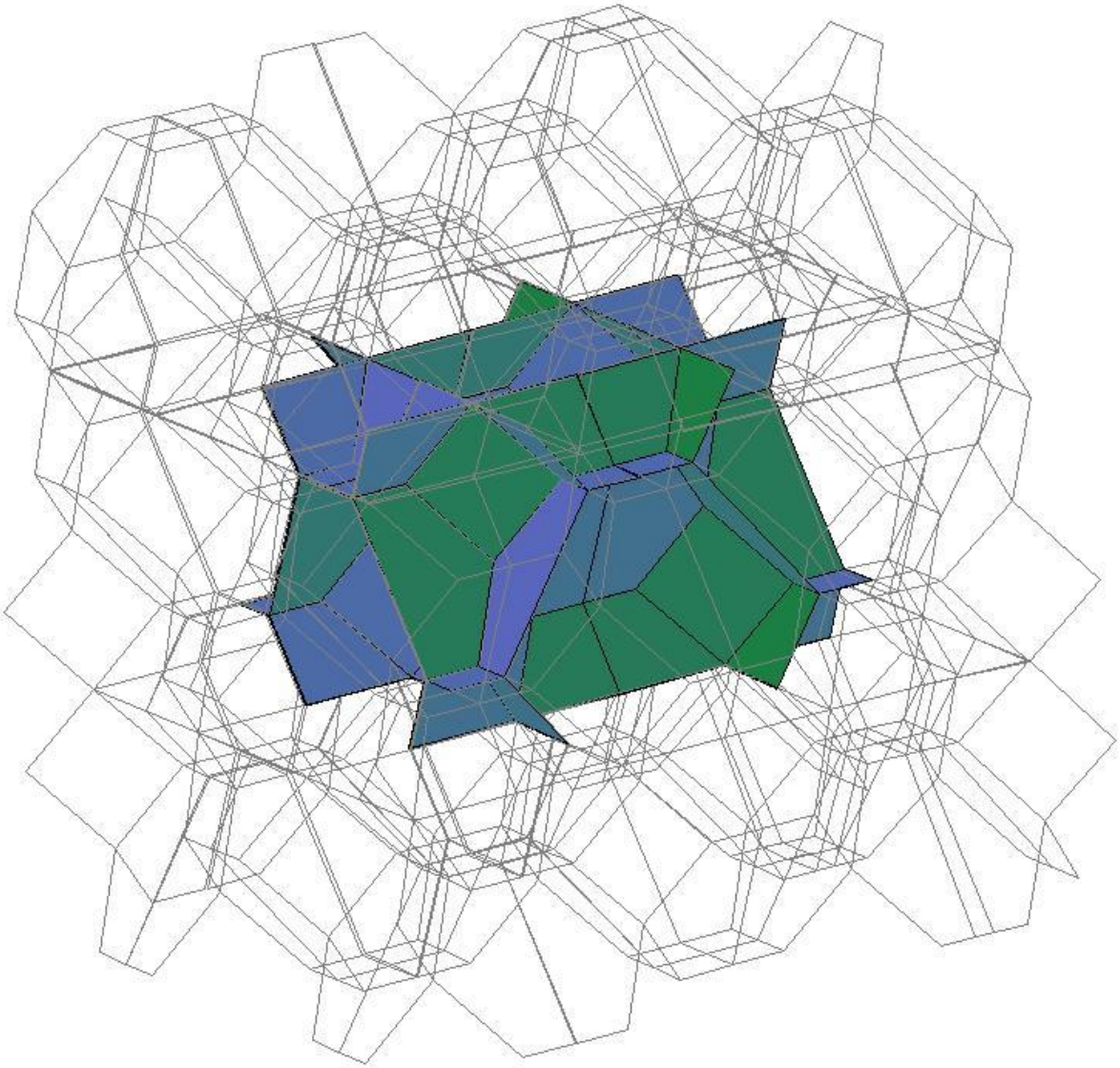

Figure 5 TKD foam with RUC highlighted

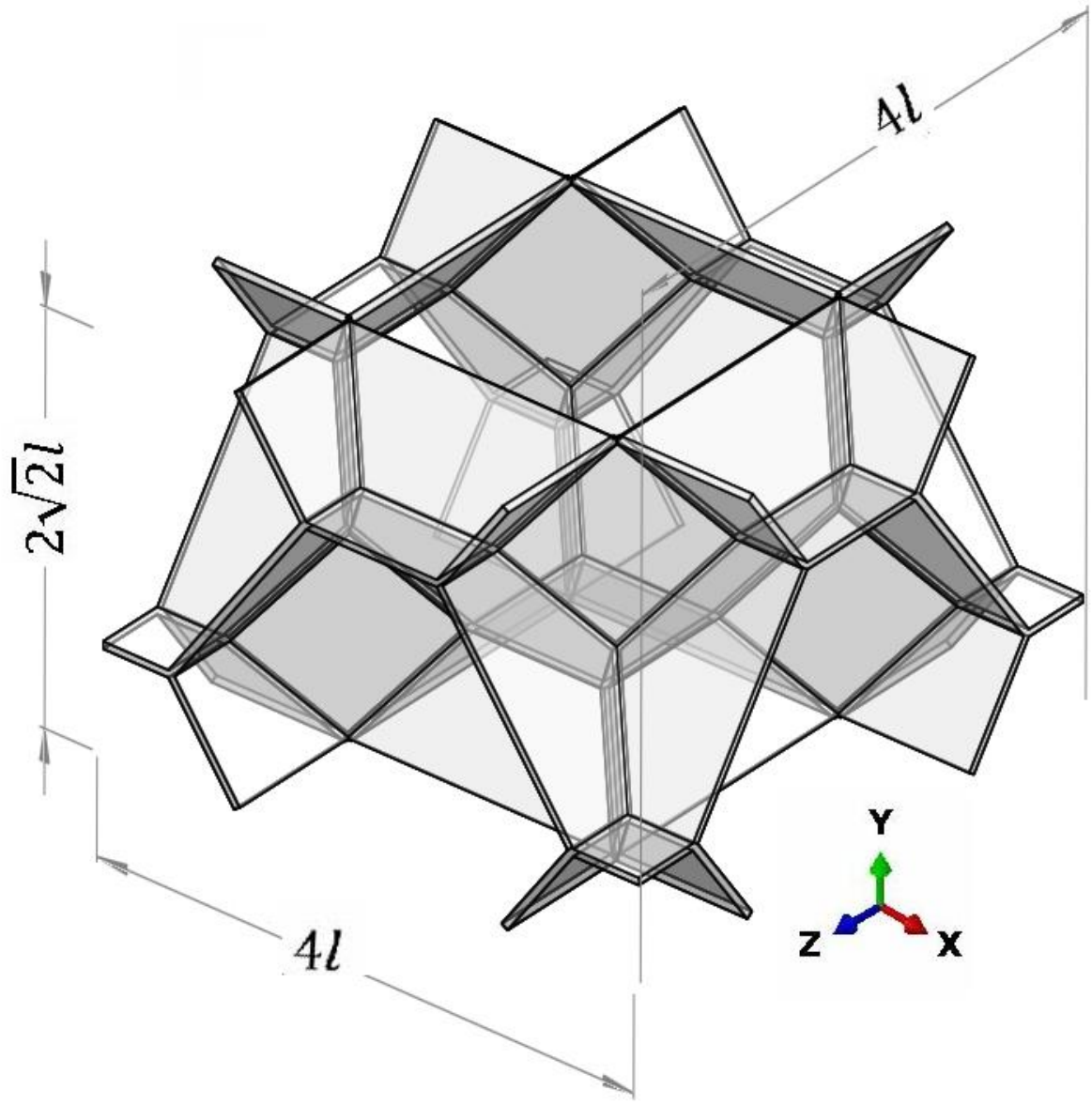

Figure 6 RUC used in FE models of Al foam

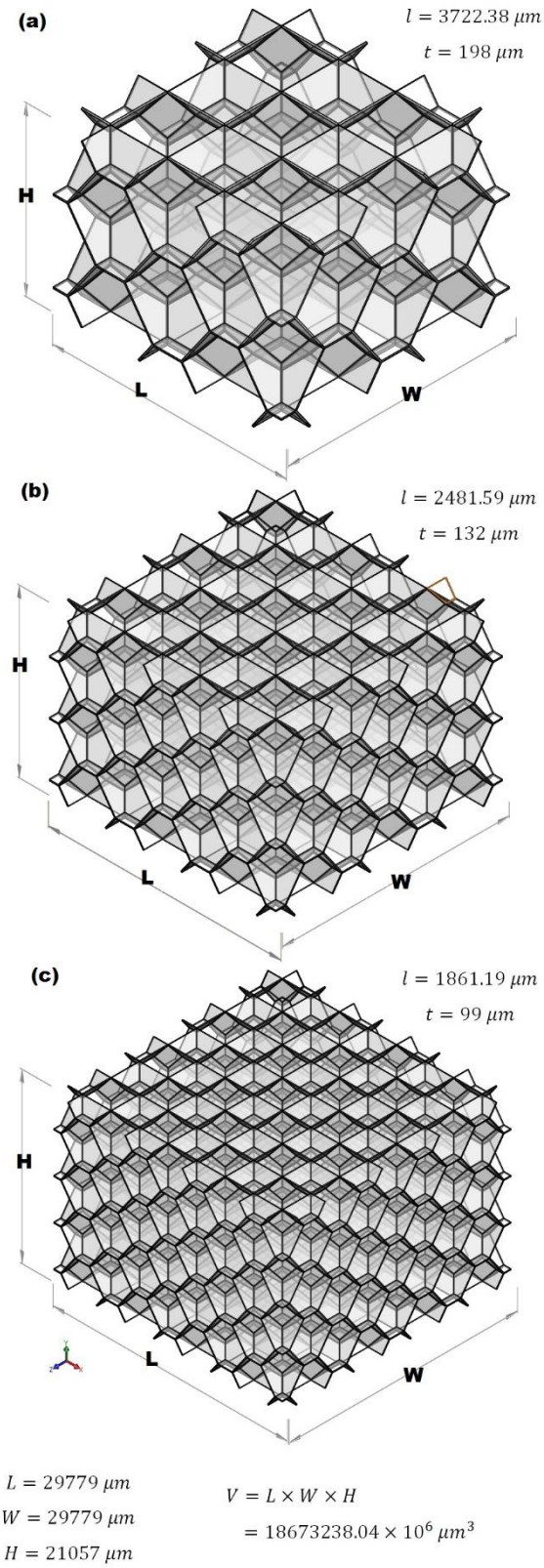

Figure 7: Aggregates of (a) 8 large (b) 27 medium and (c) 64 small RUCs of TKD foam

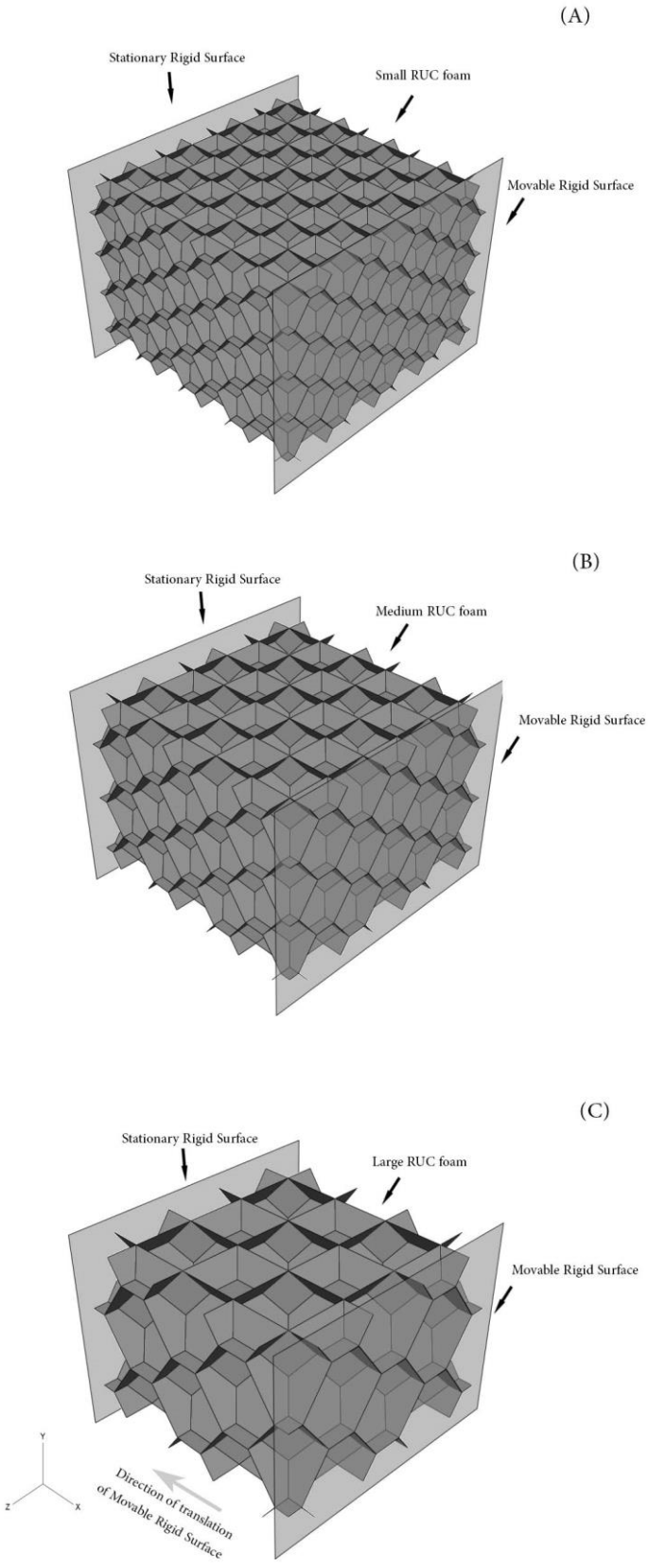

Figure 8: Crush set-up for aggregates of (a) 64 small (b) 27 medium and (c) 8 large RUCs for x directional loading

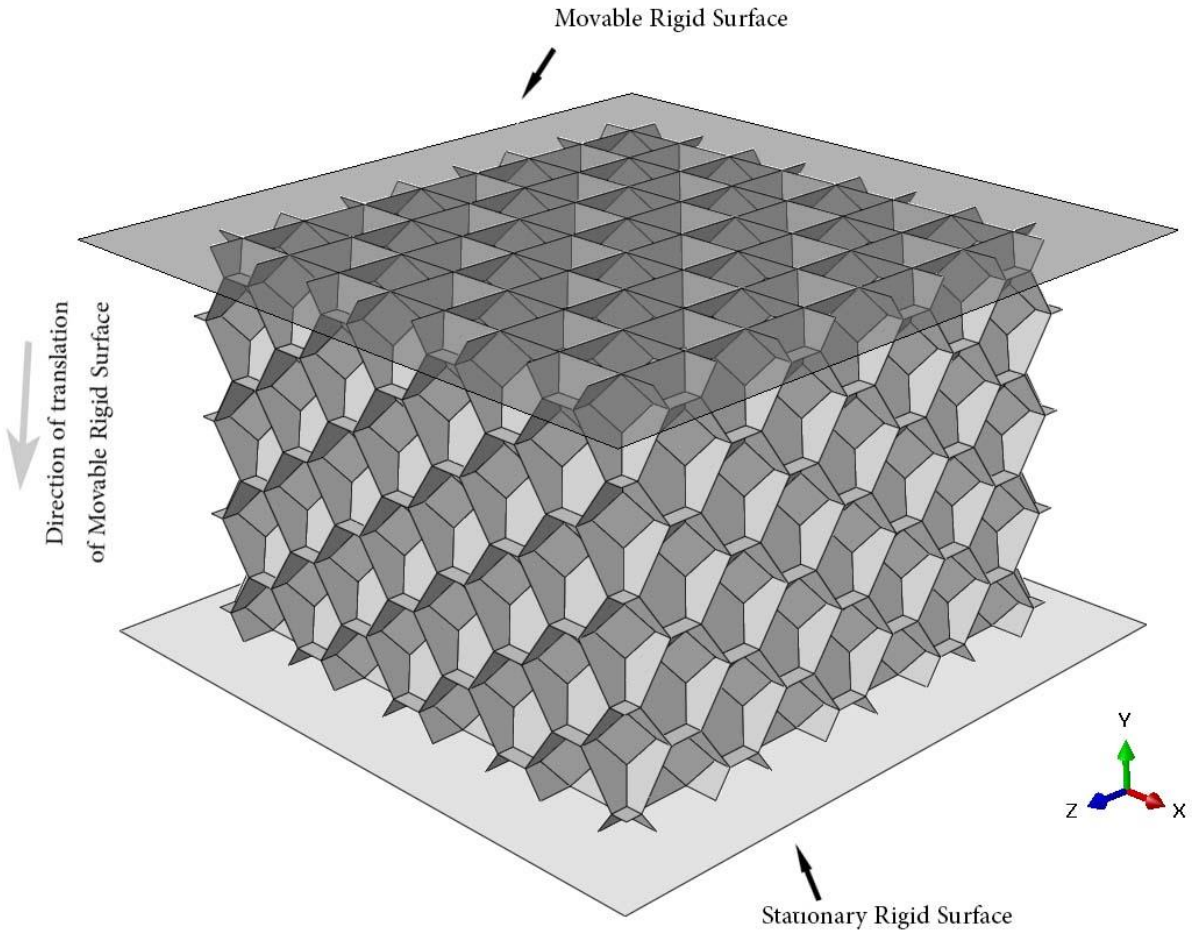

Figure 9: Simulation set-up for aggregate of 64 small RUCs for y directional loading

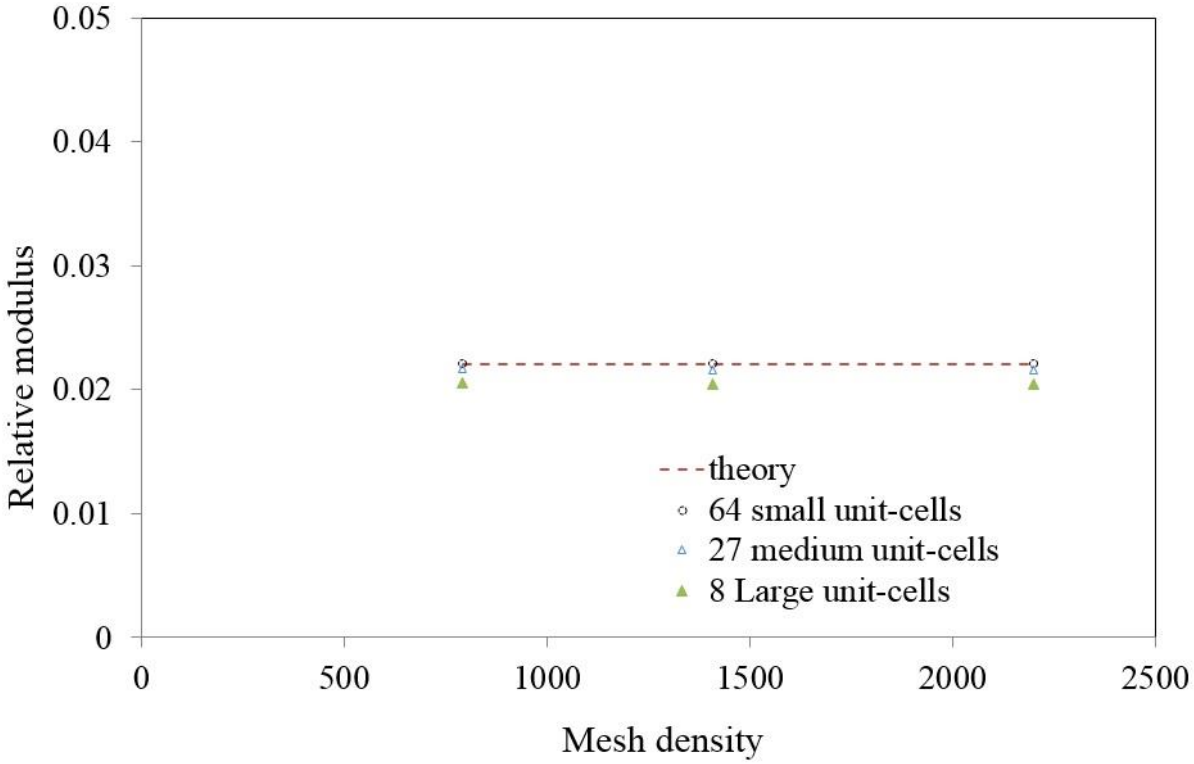

Figure 10: Verification of FE model results

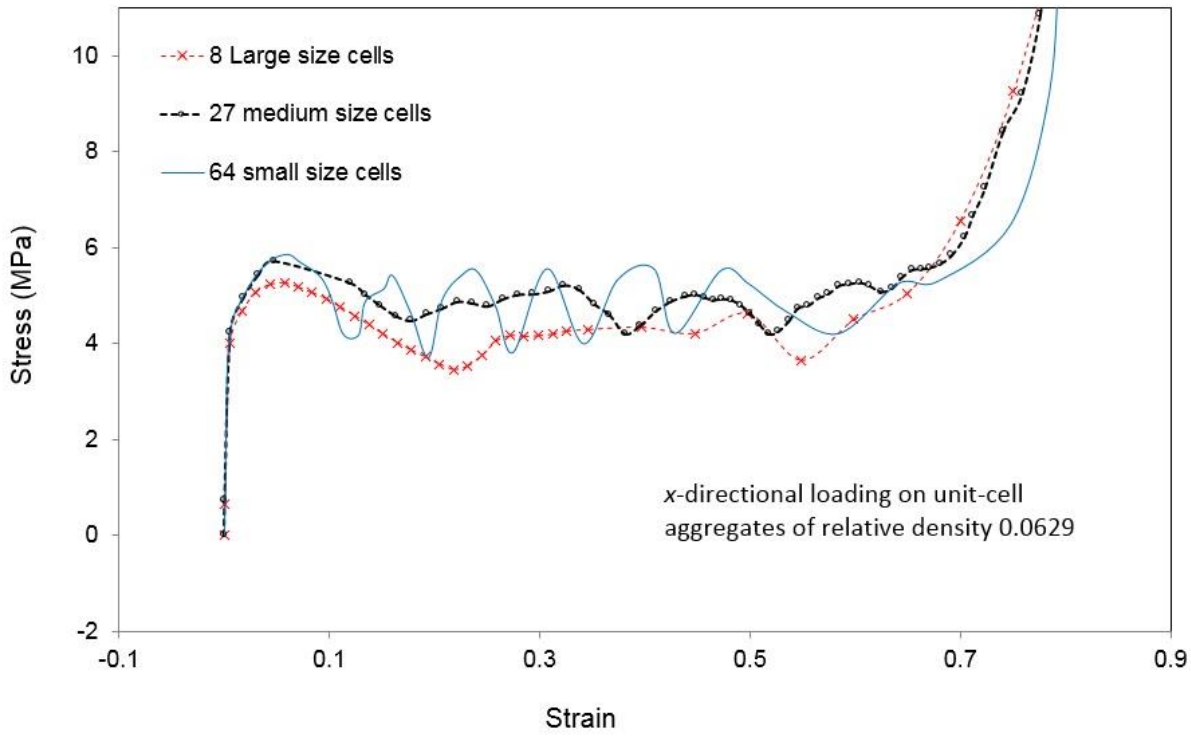

Figure 11: Compressive responses of all three cell-size RUC foams

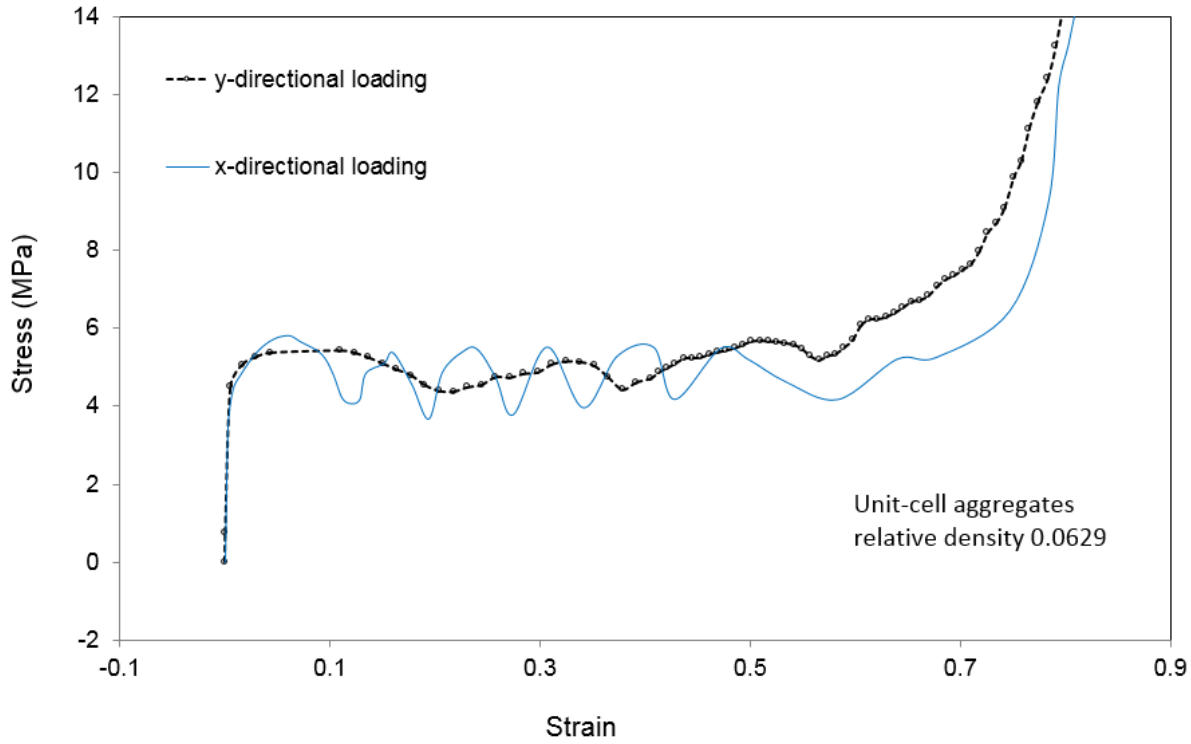

Figure 12: Compressive responses in both x and y directional loading

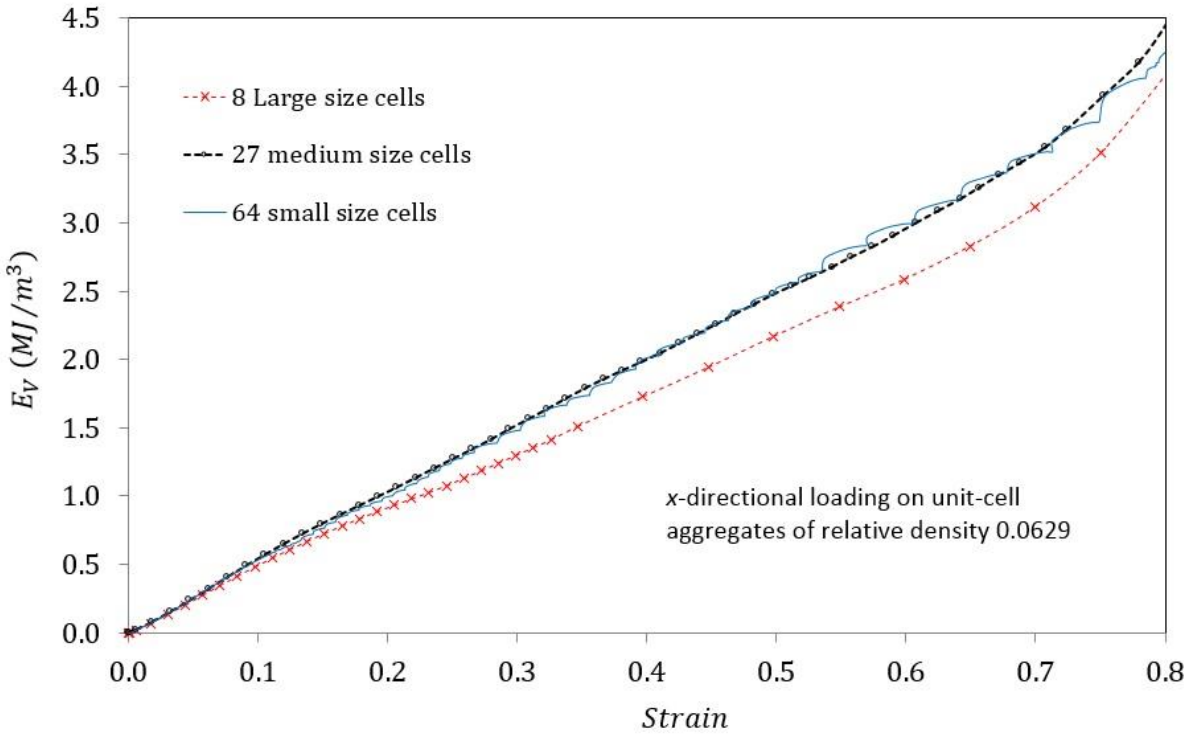

Figure 13: Energy absorbed per unit-volume of FE models for x-directional loading

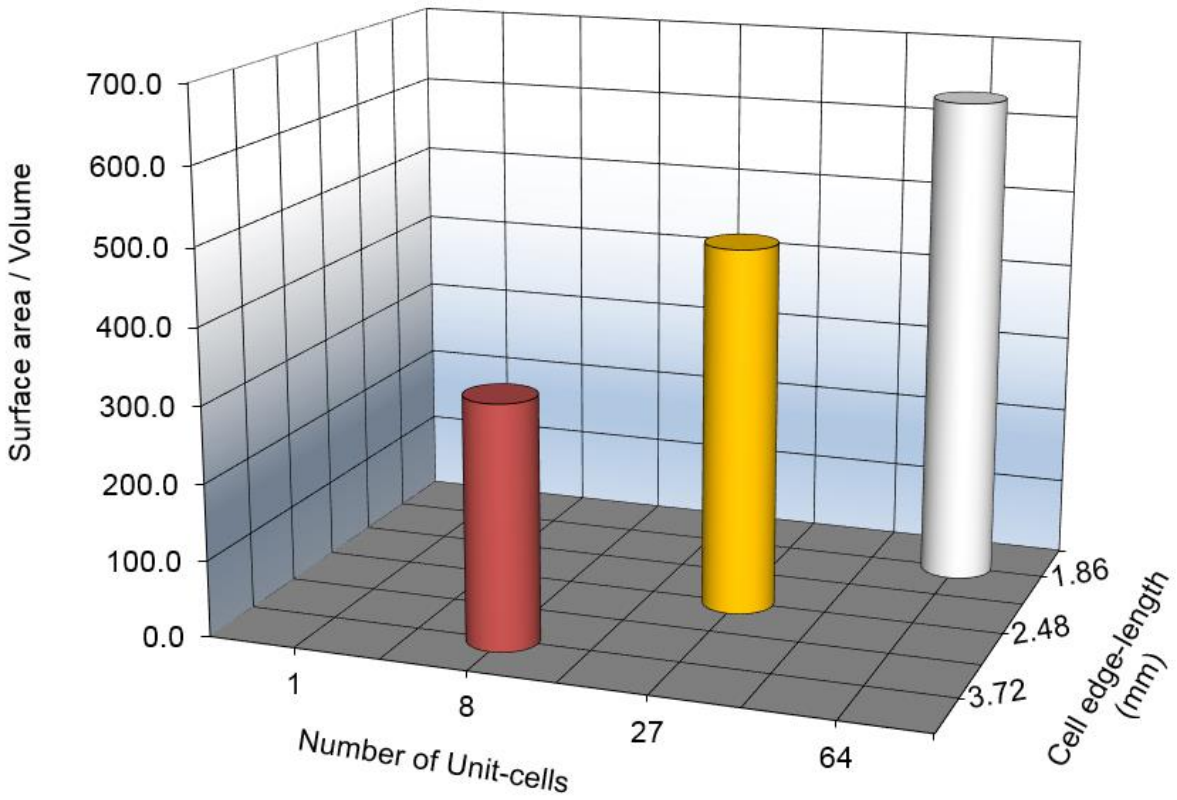

Figure 14: Surface area to volume ratio as a function of cell-size and number of cells

Density (kg/m^3)	2700
Poisson's ratio	0.3
Young's modulus (GPa)	71.0
Strain Hardening data	
Plastic-stress (MPa)	Plastic-strain
145.7	0.0
146.4	0.684×10^{-03}
152.2	0.533×10^{-02}
159.7	0.918×10^{-02}
164.0	0.116×10^{-01}
186.4	0.216×10^{-01}
236.8	0.525×10^{-01}
282.8	0.910×10^{-01}
300.6	0.114
312.7	0.134
326.1	0.151
344.2	0.192

Table 1: Material properties of AA5182